

On the area swept by a biased diffusion till its first-exit time: Martingale approach and gambling opportunities

Yonathan Sarmiento,^{1,2} Debraj Das,¹ and Édgar Roldán^{1,*}

¹*ICTP – The Abdus Salam International Centre for Theoretical Physics, Strada Costiera 11, Trieste 34151, Italy*

²*International School for Advanced Studies (SISSA), Via Bonomea 265, Trieste 34136, Italy*

Using martingale theory, we compute, in very few lines, exact analytical expressions for various first-exit-time statistics associated with one-dimensional biased diffusion. Examples include the distribution for the first-exit time from an interval, moments for the first-exit site, and functionals of the position, which involve memory and time integration. As a key example, we compute analytically the mean area swept by a biased diffusion until it escapes an interval that may be asymmetric and have arbitrary length. The mean area allows us to derive the hitherto unexplored cross-correlation function between the first-exit time and the first-exit site, which vanishes only for exit problems from symmetric intervals. As a colophon, we explore connections of our results with gambling, showing that betting on the time-integrated value of a losing game it is possible to design a strategy that leads to a net average win.

Keywords: Martingale theory, First-passage processes, Brownian motion

I. INTRODUCTION

The genesis of research in stochastic processes can be traced back to at least 1827, when Robert Brown [1] observed the erratic movements of pollen grains suspended in water, later termed Brownian motion. The phenomenon remained unexplained until Einstein in 1905 [2] developed a microscopic theory for the diffusive motion of Brownian particles, first tested in the lab by Perrin [3]. Since then, Brownian motion, often referred to as diffusion, has become a key model for investigating diverse phenomena related to stochastic processes across various scientific disciplines, such as physics, chemistry, biology, and mathematics, as well as in economics, finance, and computer science. It has helped in many fundamental advancements of equilibrium and nonequilibrium statistical physics [4, 5], fluid mechanics [6, 7], probability theory and stochastic differential equations [8–10]. Diffusion has also played a central role in studies of option pricing in finance [11], microrheology of viscoelastic materials [12], quantum fluctuations [13, 14], etc. One aspect of diffusion that has emerged as a topic of recent interest is the statistics of area-like functionals covered by a Brownian trajectory [15–18]. Specifically, such studies discover numerous practical uses in the fields of physics, mathematics, and computer science [19]. Examples range from determining the expenses involved in building a table for data storage through linear probing with a random hashing algorithm [20], analyzing statistics related to the maximal relative height of fluctuating interfaces [15] to studying various discrete combinatorial problems found in graph theory that are associated with Bernoulli processes [21].

In the last century, the development of the theory of stochastic processes has provided means to quantify a

plethora of statistical properties of nonequilibrium processes driven by Brownian noise, such as that induced by thermal fluctuations. Such efforts paved the way, among other things, to the introduction of the mathematical foundations for what is now known today as martingales [22]. Martingales, stochastic processes that serve as unbiased predictors of the future, become a key building block and also may provide a robust framework for understanding the dynamics of Brownian motion. In the context of nonequilibrium physics, martingales have found a recent revival leading to a novel ‘martingale’ formalism for stochastic thermodynamics [23]. This formalism has brought a plethora of exact results concerning various quantities, e.g., stopping-time and extreme-value statistics of thermodynamic quantities [23]. One of the most important aspects of the martingale approach is that it makes the computation of averages of relevant quantities readily approachable. For example, by choosing an appropriate function, we may compute the mean area under the curve of a path that follows a Brownian motion with a directional bias. Previous works have explored this problem for a single absorbing boundary using techniques such as path-integral methods [16, 17, 21, 24].

Interesting recent papers about the stochastic area and universal first-passage statistics have provided insights into various aspects of stochastic processes. Studies on planar Brownian motion and linear ergodic diffusions have contributed to our understanding of stochastic areas, including the generation function, large deviation functions, and asymptotic properties [25]. Additionally, the existence of anomalous scaling behavior has been found in the fluctuations of the area swept by one-dimensional Brownian motion, revealing deviations from traditional large deviations principles and uncovering singularities indicative of dynamical phase transitions [26]. On the other hand, the theory of first-passage [27, 28], which may also be realized as a sink of probability and be tackled by using probability flow analysis [29], has practical applications and relevance in

* edgar@ictp.it

various fields, e.g., in constraints arising in nonequilibrium thermodynamics [30], in the ranking of influential nodes in networks [31], etc. Furthermore, a bi-scaling theory has been proposed for first-passage times in confined compact processes, offering a comprehensive framework for understanding the probability density across different time scales [32].

In this work, we focus on the statistics of one-dimensional biased diffusion X_t which follow the overdamped Langevin equation

$$\dot{X}_t = v + \sqrt{2D}\xi_t, \quad (1)$$

where $\xi_t = \dot{B}_t$ is the standard Gaussian white noise with zero mean $\langle \xi_t \rangle = 0$ and autocorrelation function $\langle \xi_t \xi_{t'} \rangle = \delta(t - t')$. Here, v is the drift velocity, which we will often take $v \geq 0$, and $D > 0$ is the diffusion coefficient. We will assume that the initial position of the biased diffusion to be set at a fixed value X_0 , which we will often take to be equal to zero, thus we have $X_t = X_0 + vt + \sqrt{2D}B_t$ with B_t being the Wiener process.

We focus here on the dynamics (1) within an interval $[-l_-, l_+]$, with $l_- > 0$ and $l_+ > 0$, provided that the diffusion starts within the interval, i.e., $X_0 \in (-l_-, l_+)$. We investigate first-exit-time statistics for the biased diffusion to first reach any of two absorbing boundaries located at $-l_-$ and l_+ . In particular, we ask ourselves:

- What is the probability density $P(T)$ for the first-exit time

$$T = \inf\{t \geq 0 | X_t \notin (-l_-, l_+)\} \quad (2)$$

from the interval?

- What are the splitting probabilities P_- and $P_+ = 1 - P_-$ for the particle to first exit the interval from $-l_-$ and from l_+ , respectively?
- Are the first-exit time T and the first-exit position, i.e., the position at time T , X_T statistically correlated? Note that X_T is a binary random variable that can assume a value equal to either $-l_-$ or l_+ .
- Can one access the statistics of the *area under the stochastic curve* X_t

$$A_t = \int_0^t ds X_s, \quad (3)$$

in the time interval $[0, t]$? Equation (3) gives the net area under the trajectory $X_{[0,t]}$ above the time axis. In other words, A_t is a random variable that may also have negative values when the area swept by X_t below zero exceeds the area swept above zero. For an illustration, see Fig. 1, where the red and blue shaded regions under the trajectory $X_{[0,T]}$ show positive and negative contributions to A_T with T being the first-exit time.

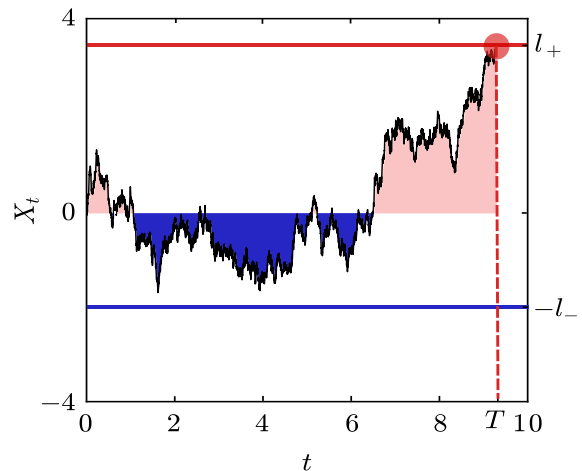


FIG. 1. Sketch of a biased diffusion X_t given by Eq. (1) with positive drift $v > 0$. The process stops at a stochastic time T given by the earliest time when the biased diffusion reaches either of two absorbing boundaries l_+ or $-l_-$. The black line depicts an example trajectory hitting the boundary l_+ at time T , which denotes the stopping time. The shaded colors illustrate the area swept by the process, with red color indicating positive contributions and blue color indicating negative ones.

Herein, we employ tools from the martingale theory to tackle all the aforementioned questions. First, we retrieve well-known analytical results in first-passage theory through rather shorter calculations than using traditional approaches (e.g. path integrals, backward Fokker-Planck equations, image method, etc.). Moreover, we establish relations between moments and cross-correlations of T and X_T which are valid for a broad class of *stopping times* which includes first-exit times as specific cases. Finally, we derive an analytical expression for the mean value of the area swept by a biased diffusion until its first-exit time from an arbitrary interval, which generalizes results from previous work [16].

II. RUDIMENTS ON MARTINGALE THEORY

We serve here an appetizer on martingale theory, reviewing known results for the ease of readers that may not be familiar with such concepts. We focus on a few well-known results that are applicable to our study, and refer readers to the recent treatise on “Martingales for physicists” [23] for further details.

A. Martingales, Submartingales and Doob’s optional stopping theorem

To warm up, we recall well-known statistical properties of diffusion. It is well known that a biased diffusion (1) with positive drift $v \geq 0$ is a *submartingale*, i.e., its con-

ditional average obeys

$$\langle X_t | X_{[0,s]} \rangle \geq X_s, \quad (4)$$

which holds for any given past history $X_{[0,s]} \equiv \{X_{t'}\}_{t' \in [0,s]}$ with $0 \leq s \leq t$. In other words, their average conditionally increases with time. For unbiased diffusions $v = 0$, one retrieves that the Wiener process is a *martingale*, i.e.,

$$\langle B_t | B_{[0,s]} \rangle = B_s, \quad (5)$$

for any given past history $B_{[0,s]}$ and $0 \leq s \leq t$. In other words, unbiased diffusions represent “fair games” which neither increase nor decrease conditionally with time.

Central results in martingale theory are Doob’s optional stopping theorems [22] (see Ch.4 in [23]). When applied to biased diffusion (1) with $v \geq 0$, and fixed initial condition X_0 , the following version of Doob’s optional stopping theorem for submartingales (OSTs) holds,

$$\langle X_T \rangle \geq X_0. \quad (6)$$

Here, T is a *stopping time* which is the first time X_t satisfies a predefined criterion. The average $\langle X_T \rangle$ is done over the values that X_t takes at time T when the criterion is first met. Remarkably, the OSTs (6) holds for a broad class of stopping times as long as two conditions are met:

I. The long-time limit of the survival probability associated with T vanishes, i.e., $P(T < \infty) = 1$; and

II. X_t is bounded at the stopping time, i.e., $|X_T| < \infty$.

The inequality (6) indicates that all stopping rules obeying these two criteria lead to an average *gain* with respect to the initial value of the process. For unbiased diffusion $v = 0$, Eq. (6) becomes Doob’s optional stopping theorem for martingales (OSTm)

$$\langle X_T \rangle = X_0, \quad (7)$$

which holds for any martingale process X_t with a fixed initial value X_0 , see Ch. 4 in the Review [23]. In other words, martingales are *fair games* leading to no net gain or loss with respect to their initial value.

The Wiener process $B_t = X_t - vt$ illustrates that one can construct a martingale from a submartingale. As we review in Sec. II B, it is possible to systematically construct parametric families of martingales associated with submartingales. Such martingales are often written as functionals of X_t and can be used, as we will show later, to extract analytical expressions for various first-exit-time statistics through the OSTm (7). In particular, for biased diffusions, the first-exit time from a finite interval and the first-passage time to reach a single threshold in the direction of the drift are two suitable examples of T , for which we can apply fruitfully the OSTm (7) as we will show from Sec. III and beyond.

B. Constructing martingales from biased diffusions

We refresh here readers about two celebrated parametric families of martingales that can be constructed using generic Markov processes as their building blocks. Particular emphasis will be given to specializing those families to the case of biased diffusion.

Doléans–Dade family. The Doléans–Dade stochastic exponential [33] associated with the Wiener process B_t , defined as $\mathcal{E}_t(z) \equiv \exp[zB_t - z^2t/2]$, is a martingale for all $z \in \mathbb{R}$ [23, 34], obeying $\langle \mathcal{E}_t(z) | B_{[0,s]} \rangle = \mathcal{E}_s(z)$ for $0 \leq s \leq t$. Such martingale, originally introduced by Catherine Doléans–Dade in the 1970s [33], is also known as the zero-drift geometric Brownian motion. Substituting the Wiener process by $B_t = (X_t - X_0 - vt)/(\sqrt{2D})$ in the Doléans–Dade exponential, one retrieves that

$$\mathcal{E}_t(z) = \exp \left[\frac{z}{\sqrt{2D}}(X_t - X_0) - \left(\frac{zv}{\sqrt{2D}} + \frac{z^2}{2} \right) t \right] \quad (8)$$

provides a class of martingale processes associated with the biased diffusion X_t . In other words, the stochastic exponential $\mathcal{E}_t(z)$ in Eq. (8) is a martingale associated with the biased diffusion X_t for all real values of the parameter $z \in \mathbb{R}$.

For the choice $z = -v\sqrt{2/D}$, we retrieve from Eq. (8) the thermodynamic martingale

$$\Sigma_t = \exp \left[-\frac{v}{D}(X_t - X_0) \right], \quad (9)$$

namely, that negative of the stochastic entropy production $S_t^{\text{tot}} = (v/D)(X_t - X_0)$ associated with the biased diffusion is an exponential martingale in time-homogeneous stationary states [35, 36]. Such result is the cornerstone of the martingale theory for stochastic thermodynamics in nonequilibrium stationary states, see [23]. As we will see in Sec. III and beyond, other choices for z in the Doléans–Dade family are instrumental for first-passage-time calculations.

Dynkin family. Eugene Dynkin [37] proved rigorously that one can systematically construct martingales associated with a generic Markov process and a function $g \equiv g_t(x)$ that may depend explicitly on t and x . In particular,

$$\mathcal{Y}_t[g] = g_t(X_t) - g_0(X_0) - \int_0^t ds [\partial_s g_s(X_s) + \mathcal{L}g_s(X_s)] \quad (10)$$

constitutes a martingale with respect to X_t for any family of real-valued, smooth bounded function $g_t(x)$, for which the derivatives $\partial_t g_t(x)$, $\partial_x g_t(x)$, and $\partial_x^2 g_t(x)$ exist [23]. Here \mathcal{L} denotes the generator of the Markov process X_t at time t , for which its instantaneous density $\rho_t(x)$ follows $\partial_t \rho_t(x) = \mathcal{L}^\dagger \rho_t(x)$, where \mathcal{L}^\dagger is the adjoint of the operator \mathcal{L} . When specialized over biased diffusion (Eq. (1)), we have $\mathcal{L}^\dagger = -v\partial_x + D\partial_x^2$ and $\mathcal{L} = v\partial_x + D\partial_x^2$, and therefore,

Dynkin's martingales read

$$\begin{aligned} \mathcal{Y}_t[g] &= g_t(X_t) - g_0(X_0) \\ &\quad - \int_0^t ds \left[(\partial_s g_s + v \partial_x g_s + D \partial_x^2 g_s)(X_s) \right], \end{aligned} \quad (11)$$

and obey $\langle \mathcal{Y}_t[g] | X_{[0,s]} \rangle = \mathcal{Y}_s[g]$ for any $t \geq s \geq 0$.

C. Generic properties of stopping times for drift-diffusion dynamics

Expanding the Doléans–Dade exponential associated with B_t around z small, one may write

$$\begin{aligned} \mathcal{E}_t(z) &= 1 + zB_t + \frac{z^2}{2!}(B_t^2 - t) + \frac{z^3}{3!}(B_t^3 - 3tB_t) + \dots, \\ &= \sum_{n=0}^{\infty} \frac{z^n}{n!} H_t^{(n)}, \end{aligned} \quad (12)$$

and show that the stochastic processes in the expansion (12), which we denote by $H_t^{(n)}$, are all martingales satisfying $\langle H_t^{(n)} | B_{[0,s]} \rangle = H_s^{(n)}$ for all $t \geq s \geq 0$ and for all $n \geq 0$ [23]. Here, the martingales $H_t^{(n)}$ can be written in the form of Hermite polynomials evaluated over realizations of the Wiener process as

$$H_t^{(n)} = (-t)^n \exp\left(\frac{B^2}{2t}\right) \frac{d}{dB^n} \exp\left(-\frac{B^2}{2t}\right) \Big|_{B=B_t}. \quad (13)$$

Considering the $n = 1$ martingale defined with respect to the drift-diffusion process, we may write $H_t^{(1)} = B_t = (X_t - X_0 - vt)/(\sqrt{2D})$. Then, applying Doob's OSTm (7) to the martingale $H_t^{(1)}$, i.e., $\langle H_T^{(1)} \rangle = H_0^{(1)} = 0$, we get $\langle (X_T - X_0 - vT) \rangle / (\sqrt{2D}) = H_0^{(1)} = 0$, which leads to the mean stopping time:

$$\langle T \rangle = \frac{\langle X_T \rangle - X_0}{v}. \quad (14)$$

Similarly, applying the OSTm (7) to higher-order martingales $H_t^{(n)}$, one finds the ($n \geq 2$)-th moments of the stopping time for the drift-diffusion process. For example, we obtain from $H_t^{(2)} = B_t^2 - t$ and $H_t^{(3)} = B_t^3 - 3tB_t$ that

$$\langle T^2 \rangle = \frac{X_0^2 - \langle X_T^2 \rangle}{v^2} + \frac{2 \langle X_T T \rangle}{v} + \frac{2D \langle T \rangle}{v^2}, \quad (15)$$

and

$$\begin{aligned} \langle T^3 \rangle &= \frac{\langle X_T^3 \rangle - X_0^3}{v^3} - \frac{3}{v^2} \langle X_T^2 T \rangle + \frac{3}{v} \langle X_T T^2 \rangle \\ &\quad - \frac{3X_0}{v^3} \langle X_T^2 \rangle + \frac{3}{v^2} (2D - vX_0) \langle T^2 \rangle \\ &\quad + \frac{6}{v^3} (vX_0 - D) \langle X_T T \rangle + \frac{3X_0^2}{v^3} \langle X_T \rangle \\ &\quad + \frac{3X_0}{v^3} (2D - vX_0) \langle T \rangle, \end{aligned} \quad (16)$$

respectively. Equations (15) and (16) reveal that computing ($n > 1$)-th moment of the stopping time T requires *in general* the knowledge of the cross correlations $\langle X_T^m T^n \rangle$.

D. First-exit-site distribution for asymmetric intervals

For the most generic case with two absorbing boundaries at $-l_-$ and l_+ with $l_{\pm} > 0$, the stopping time T is given by the first-exit time from the interval $(-l_-, l_+)$, i.e., one has $T = \inf\{t \geq 0 | X_t \notin (-l_-, l_+)\}$. Consequently, at the stopping time T , the position of the particle X_T becomes a binary random variable that takes two possible values $-l_-$ and l_+ , and thus the first-exit-site distribution is given by

$$P(X_T) = P_+ \delta_{X_T, l_+} + P_- \delta_{X_T, -l_-}, \quad (17)$$

where $\delta_{i,j}$ denotes Kronecker's delta. We thus denote in the following the probabilities of X_T taking on the values $-l_-$ and l_+ by $P_- \equiv P(X_T = -l_-)$ and $P_+ \equiv P(X_T = l_+)$, respectively.

Applying Doob's optional stopping theorem to the martingale Σ_t defined in Eq. (9), we get $\langle \exp(\Sigma_T) \rangle = 1$, i.e.,

$$\begin{aligned} \underbrace{\langle \exp\left[-\frac{v}{D} X_T\right] \rangle}_{P_+ \exp(-vl_+/D) + P_- \exp(vl_-/D)} &= \exp\left[-\frac{vX_0}{D}\right], \end{aligned} \quad (18)$$

which together with the normalization condition $P_+ + P_- = 1$ yields

$$\begin{aligned} P_- &= \frac{\exp[-v(l_- + X_0)/D] - \exp[-v(l_- + l_+)/D]}{1 - \exp[-v(l_- + l_+)/D]}, \\ P_+ &= \frac{1 - \exp[-v(l_- + X_0)/D]}{1 - \exp[-v(l_- + l_+)/D]}. \end{aligned} \quad (19)$$

The m -th moment of X_T is given by

$$\langle X_T^m \rangle = (-l_-)^m P_- + l_+^m P_+. \quad (20)$$

Substituting Eq. (20) for $m = 1$ in Eq. (14) we find that the mean exit time reads

$$\langle T \rangle = \frac{l_+ P_+ - l_- P_- - X_0}{v}. \quad (21)$$

Similarly, the n -th moment of the first-exit time T is given by

$$\langle T^n \rangle = P_- \langle T^n | X_T = -l_- \rangle + P_+ \langle T^n | X_T = l_+ \rangle, \quad (22)$$

where the moments $\langle T^n | X_T = -l_- \rangle$ and $\langle T^n | X_T = l_+ \rangle$ are to be computed with respect to the conditional probabilities $P(T | X_T = -l_-)$ and $P(T | X_T = l_+)$, respectively. Furthermore, the cross-correlations between the exit time and the exit site read

$$\begin{aligned} \langle X_T^m T^n \rangle &= P_- (-l_-)^m \langle T^n | X_T = -l_- \rangle \\ &\quad + P_+ l_+^m \langle T^n | X_T = l_+ \rangle. \end{aligned} \quad (23)$$

We remark that X_T and T are in general correlated random variables, which implies that it is highly non-trivial to compute $\langle T^n \rangle$ and $\langle X_T^m T^n \rangle$ through Eqs. (22) and (23). As we will show in the next Sec. II E, such calculations can be enormously simplified for the specific case of a exit-time problem from a symmetric interval around the origin.

E. First-exit-time symmetry for symmetric intervals

For symmetric thresholds $l_+ = l_- = l$ about an initial condition $X_0 = 0$, it was shown that the following first-passage-time symmetry

$$P(T|X_T = l) = P(T|X_T = -l), \quad (24)$$

holds [23, 38–41]. Equation (24) implies that in case of symmetric thresholds the statistics of the trajectories that reach the positive threshold l is the same as that of the trajectories that reach the negative threshold $-l$. We remark that this result holds even in presence of a non-zero drift. In other words, one may say that for symmetric thresholds even with $v \neq 0$ the distributions of the first-passage time for trajectories reaching either l or $-l$ are the same. Consequently, the first-passage symmetry (24) also implies that the conditional density of the escape time obeys

$$P(T|X_T) = P(T). \quad (25)$$

Therefore, for symmetric intervals, the mutual information between the exit time and the exit site vanishes

$$I(X_T : T) = \left\langle \log \frac{P(T, X_T)}{P(T)P(X_T)} \right\rangle = 0, \quad (26)$$

thus the random variables X_T and T are uncorrelated. Equation (26) was mathematically proven in Ref. [40] in context of binary sequential hypothesis testing with symmetric error probabilities. More precisely, Corollary 2 in [40] implies Eq. (26) for the specific example of a binary decision among two hypotheses: H_0 the dynamics is governed by $\dot{X}_t = v + \sqrt{2D}\xi_t$, and H_1 the dynamics is governed by $\dot{X}_t = -v + \sqrt{2D}\xi_t$, see also [41] for further details.

Interestingly, condition (26) implies that the cross-correlation function between the exit site and the exit time vanishes, i.e.,

$$C(X_T, T) = \langle X_T T \rangle - \langle X_T \rangle \langle T \rangle = 0, \quad (27)$$

and similarly the cross-correlation function of arbitrary powers is given by

$$C(X_T^m, T^n) = \langle X_T^m T^n \rangle - \langle X_T^m \rangle \langle T^n \rangle = 0, \quad (28)$$

for any integer m and n . Equation (28) is instrumental to obtain analytical expressions for the n -th moment of

the first-exit time from a symmetric interval around the origin. This can be easily grasped by noting that for symmetric intervals with $X_0 = 0$ one has (see Eqs. (20) and (21))

$$\langle X_T^m \rangle = \begin{cases} l^m & \text{for } m \text{ even,} \\ l^{m-1} v \langle T \rangle & \text{for } m \text{ odd,} \end{cases} \quad (29)$$

and then by using $\langle X_T^m T^n \rangle = \langle X_T^m \rangle \langle T^n \rangle$ in Eqs. (15)–(16), which reveals that the n -th moments (with arbitrary $n > 1$) of the exit time can be expressed in terms of simple functions of solely the first moment $\langle T \rangle$.

III. FIRST-PASSAGE STATISTICS

A. Single absorbing boundary

Let us now choose a stopping criterion for the process X_t . Suppose the process starts at $X_0 = 0$, there is an absorbing boundary at $l > 0$, and the process stops as soon as it reaches the absorbing boundary. The stopping time T in this case is defined by

$$T \equiv \inf\{t \geq 0 | X_t \geq l\}, \quad (30)$$

which is nothing but the first-passage time to the absorbing boundary l . The first-passage properties of a drift-diffusion process are well-studied in the literature. Arguably, the method of images may be considered as one of the simplest approach to obtain closed-form solutions for the probability density $P(T)$ of the stopping time T and survival probability $S(t)$ at a given time t [27]. However, in the following, we show how one may obtain the results in an elegant way by using the Martingale theory. This method often referred to as the Gerber–Shiu technique helps in computing the Laplace transforms of probability densities of stopping times using martingale properties and has been used in mathematical finance [42], mathematical psychology [43], stochastic thermodynamics [44], etc.

In order to obtain the density $P(T)$, we recall that the Doléans-Dade exponential $\mathcal{E}_t(z)$ defined in Eq. (8) is a martingale and satisfies $\mathcal{E}_0 = 1$. Then, applying Doob's OSTm (7) to this martingale, we obtain $\langle \mathcal{E}_T \rangle = \mathcal{E}_0 = 1$, which implies the exact relation

$$\left\langle \exp \left[- \underbrace{\left(\frac{zv}{\sqrt{2D}} + \frac{z^2}{2} \right)}_s T \right] \right\rangle = \exp \left(- \frac{zl}{\sqrt{2D}} \right), \quad (31)$$

where we have used the fact that $X_T = l$. Equation (31) provides a direct route to the Laplace transform of the first-exit-time probability density $P(T)$ as $\tilde{P}(s) \equiv \mathcal{L}[P(T)](s) = \langle \exp(-sT) \rangle = \int_0^\infty dT \exp(-sT) P(T)$ with $s > 0$. To obtain the time-dependent probability density, we reparametrize the argument of the exponential in the left-hand-side of Eq. (31) using the relation

$s(z) = zv/\sqrt{2D} + z^2/2$, and compute its roots $z_{\pm}(s) \equiv (-v \pm \sqrt{v^2 + 4Ds})/(\sqrt{2D})$, from which only the positive root z_+ gives us $s > 0$ for $v > 0$. By specializing z in to the positive root, i.e., substituting

$$z = \frac{-v + \sqrt{v^2 + 4Ds}}{\sqrt{2D}}, \quad (32)$$

in the right-hand side of Eq. (31), one identifies its left-hand side as the Laplace transform of the first-exit-time distribution, which reads

$$\tilde{P}(s) = \exp\left(\frac{vl - l\sqrt{v^2 + 4Ds}}{2D}\right). \quad (33)$$

Performing the inverse Laplace transform we obtain from Eq. (33) the probability density of the stopping time [27]

$$\begin{aligned} P(T) &= \mathfrak{L}^{-1}[\tilde{P}(s)](T) \\ &= \frac{l}{\sqrt{4\pi DT^3}} \exp\left[-\frac{(l-vT)^2}{4DT}\right]. \end{aligned} \quad (34)$$

which was also obtained in textbook reference with, e.g., the image method [27] following rather longer calculations.

B. Two symmetric absorbing boundaries

We now consider the case with two absorbing boundaries at $-l$ and l symmetrically placed about the initial position $X_0 = 0$. Here, the process X_t stops as soon as it reaches either of the absorbing boundaries. Consequently, the first-exit time (2) from the interval $(-l, l)$ in this case is given by

$$T = \inf\{t \geq 0 | X_t \notin (-l, l)\}. \quad (35)$$

Unlike the case of a single absorbing boundary, here the exit site $X_T = \{l, -l\}$ becomes a binary random variable with probability distribution $P(X_T) = P_+ \delta_{X_T, l} + P_- \delta_{X_T, -l}$, where P_+ and $P_- = 1 - P_+$ are the absorption probabilities at sites l and $-l$, respectively. Despite this additional complexity, we can crack key first-exit-time statistics in few lines using martingales.

To derive the density $P(T)$ of the first-exit time (35), we follow analogous steps as in the previous Sec. III A. The first-exit time (35) is yet another example of stopping time for which Doob's OSTm (7) applies. Specializing again the OSTm (7) to the Doléans-Dade exponential $\mathcal{E}_t(z)$ defined in Eq. (8), we obtain $\langle \mathcal{E}_T \rangle = \mathcal{E}_0 = 1$, which in this case reads

$$\left\langle \exp\left[\frac{zX_T}{\sqrt{2D}} - \left(\frac{zv}{\sqrt{2D}} + \frac{z^2}{2}\right)T\right]\right\rangle = 1. \quad (36)$$

Evaluating the average on the left-hand side of Eq. (36) is far from straightforward for generic exit times, as it requires knowledge on the joint distribution $P(X_T, T)$.

However, for the first-exit time from a symmetric interval the exit site X_T and first-exit time T are statistically independent [see Sec. II E]. As a result, the left-hand side of Eq. (36) factorizes

$$\begin{aligned} &\left\langle \exp\left[\frac{zX_T}{\sqrt{2D}} - \left(\frac{zv}{\sqrt{2D}} + \frac{z^2}{2}\right)T\right]\right\rangle \\ &= \left\langle \exp\left[\frac{zX_T}{\sqrt{2D}}\right]\right\rangle \left\langle -\left(\frac{zv}{\sqrt{2D}} + \frac{z^2}{2}\right)T\right\rangle. \end{aligned} \quad (37)$$

In the right-hand side of Eq. (37), the first average is done with respect to the first-exit-site distribution $P(X_T)$, whereas the second average is to be computed with respect to the first-exit-time distribution $P(T)$. Combining Eq. (36) with Eq. (37), we obtain

$$\left\langle \exp\left[-\left(\frac{zv}{\sqrt{2D}} + \frac{z^2}{2}\right)T\right]\right\rangle = \left\langle \exp\left(\frac{zX_T}{\sqrt{2D}}\right)\right\rangle^{-1}. \quad (38)$$

Specializing $z = (-v + \sqrt{v^2 + 4Ds})/(\sqrt{2D})$ [See Eq. (32)], we obtain that the Laplace transform $\tilde{P}(s)$ of the first-exit-time probability density $P(T)$, i.e.,

$$\tilde{P}(s) = \left\langle \exp\left(\frac{zX_T}{\sqrt{2D}}\right)\right\rangle^{-1}. \quad (39)$$

The average of the exponential function on the right hand side of Eq. (39) may be obtained by using Eq. (19) in Eq. (17) with $l_+ = l_- = l$. Then, and after some algebra Eq. (39) reads

$$\tilde{P}(s) = \cosh\left(\frac{lv}{2D}\right) \operatorname{sech}\left(\frac{l\sqrt{4Ds + v^2}}{2D}\right), \quad (40)$$

which in the limit $s \rightarrow 0$, yields $\lim_{s \rightarrow 0} \tilde{P}(s) = 1$, and thus shows the normalization of $P(T)$. Noting that the inverse Laplace transform of $\operatorname{sech}(b\sqrt{s})$ is given by [45, 46]

$$\begin{aligned} \mathfrak{L}^{-1}[\operatorname{sech}(b\sqrt{s})](t) &= \frac{b}{\sqrt{4\pi t^3}} \sum_{n=-\infty}^{\infty} (-1)^n (1-2n) \\ &\times \exp\left[-\frac{b^2(2n-1)^2}{4t}\right], \end{aligned} \quad (41)$$

one may invert Eq. (40) to obtain the exit-time distribution $P(T) = \mathfrak{L}^{-1}[\tilde{P}(s)](T)$ as

$$\begin{aligned} P(T) &= \frac{l}{\sqrt{4\pi DT^3}} \cosh\left(\frac{lv}{2D}\right) \exp\left(-\frac{v^2 T}{4D}\right) \\ &\times \sum_{n=-\infty}^{\infty} (-1)^n (1-2n) \exp\left[-\frac{l^2(2n-1)^2}{4DT}\right]. \end{aligned} \quad (42)$$

For an alternative expression of $P(T)$ we refer the reader to Eq. (13) in ref. [43]. We note that in refs. [45, 46], the inverse Laplace transform of $\operatorname{sech}(b\sqrt{s})$ is mistakenly

given by $-(1/b^2)[\partial_\nu \theta_1(\nu/2|t/b^2)]_{\nu=0}$, where the Theta function $\theta_1(\nu|x)$ is defined by [45]

$$\theta_1(\nu|x) \equiv \frac{1}{\sqrt{\pi x}} \sum_{n=-\infty}^{\infty} (-1)^n \exp\left[-\frac{1}{x}\left(\nu + n - \frac{1}{2}\right)^2\right]. \quad (43)$$

However, the correct expression for the inverse Laplace transform of $\text{sech}(b\sqrt{s})$ reads $(1/b^2)[\partial_\nu \theta_1(\nu/2|t/b^2)]_{\nu=0}$. The n -th moment of the exit time T may be written in terms of $\tilde{P}(s)$ as

$$\langle T^n \rangle = (-1)^n \frac{d^n}{ds^n} \tilde{P}(s) \Big|_{s=0}, \quad (44)$$

using which along with Eq. (40), the first three moments are obtained as

$$\langle T \rangle = \frac{l}{v} \tanh\left(\frac{vl}{2D}\right), \quad (45)$$

$$\langle T^2 \rangle = 2 \langle T \rangle^2 + \frac{2D}{v^2} \langle T \rangle - \frac{l^2}{v^2}, \quad (46)$$

$$\begin{aligned} \langle T^3 \rangle &= 6 \langle T \rangle^3 + \frac{12D}{v^2} \langle T \rangle^2 + \left(\frac{12D^2}{v^4} - \frac{5l^2}{v^2}\right) \langle T \rangle \\ &\quad - \frac{6Dl^2}{v^4}. \end{aligned} \quad (47)$$

Notably, the exact expressions for the moments, Eqs. (45-47) can be obtained in few lines with the martingale approach, see Sec. II C. The fact that *all moments* of the exit time are written as functions of only its first moment $\langle T \rangle$ is a direct consequence of the fact that T and X_T are uncorrelated in the first-exit-time problem around a symmetric interval, see Sec. II E.

C. Two asymmetric absorbing boundaries

Obtaining closed-form expression for the exit-time distribution $P(T)$ in the case of asymmetric absorbing boundaries about the origin is full of challenges. Unlike the previous case with symmetric boundaries, where the exit site X_T and exit time T are statistically independent (see Sec. II E), here it is not easy to make any such comment. Consequently, the factorization in Eq. (37) that

assumes the independence of X_T and T may not be employed for asymmetric boundaries. However, as discussed in Sec II D, using the martingale approach we may obtain a closed-form expression for the mean exit time $\langle T \rangle$, see Eq. (21). The higher moments $\langle T^n \rangle$ ($n > 1$) of the exit time may be constructed from the mean $\langle T \rangle$, see Supplemental Material Sec. S1.

Despite the difficulty in obtaining $P(T)$, we remark that other non-trivial quantities can be effectively computed for the asymmetric boundaries employing the martingale approach. In this regard, a few examples are demonstrated in the next section.

IV. AREA SWEEPED TILL THE ESCAPE

Different from conventional techniques, we offer a direct approach of the problem of accessing the statistics of the stochastic area. We employ Dynkin's Martingales which enable an extension of the problem beyond a single absorbing boundary and the first-escape time as it has been treated in previous works. In particular, by setting $g_t(x) = x^2$ in Eq. (11), we may write

$$\begin{aligned} \mathcal{Y}_t[g] &= X_t^2 - X_0^2 - 2v \int_0^t ds X_s - 2D \int_0^t ds \\ &= X_t^2 - X_0^2 - 2vA_t - 2Dt, \end{aligned} \quad (48)$$

where $A_t = \int_0^t ds X_s$ is the stochastic area swept by X_t in the time interval $[0, t]$, as defined in Eq. (3). Applying Doob's OSTm to the martingale (48), we obtain that the mean area swept by the process till any stopping time T obeying conditions I and II (see Sec. II A) reads

$$\langle A_T \rangle = \frac{\langle X_T^2 \rangle - \langle X_0^2 \rangle - 2D\langle T \rangle}{2v}. \quad (49)$$

Equation (49) holds for any stopping time obeying Doob's OSTm requirements, for any given initial density $\rho_0(X_0)$, and for all values of $v > 0$.

In the following, we specialize our result (49) to T given by the first-exit time from the interval $(-l_-, l_+)$ for a drift-diffusion process starting at $X_0 = 0$ with drift velocity $v > 0$. By replacing the corresponding expressions for $\langle X_T^2 \rangle$ and $\langle T \rangle$ (see Supplemental Material Sec. S1) in Eq. (49), we obtain the formidable analytical expression

$$\langle A_T \rangle = \left(\frac{D^2}{v^3}\right) \frac{\exp(\text{Pe}^+) [\exp(\text{Pe}^-) - 1] [(\text{Pe}^+)^2 - 2\text{Pe}^+] + [\exp(\text{Pe}^+) - 1] [(\text{Pe}^-)^2 + 2\text{Pe}^-]}{2 [\exp(\text{Pe}^+ + \text{Pe}^-) - 1]}, \quad (50)$$

where

$$\text{Pe}^- = \frac{vl_-}{D}, \quad \text{and} \quad \text{Pe}^+ = \frac{vl_+}{D}, \quad (51)$$

are the two characteristic Péclet numbers of the biased diffusion in the asymmetric interval $[-l_-, l_+]$. Notably,

the analytical expression (50) reveals that the mean area till the first-exit time may be put in the scaling form

$$\langle A_T \rangle = \frac{D^2}{v^3} \Psi_A(\text{Pe}^+, \text{Pe}^-), \quad (52)$$

with

$$\begin{aligned} \Psi_A(x, y) &= \frac{\exp(x)(\exp(y) - 1)(x^2 - 2x) + (\exp(x) - 1)(y^2 + 2y)}{2(\exp(x + y) - 1)} \end{aligned} \quad (53)$$

being the scaling function. In the limit $y \rightarrow \infty$, we have $\lim_{y \rightarrow \infty} \Psi_A(x, y) = (x^2 - 2x)/2$. For the case of symmetric boundaries $l_- = l_+ = l$, Eq. (50) simplifies to

$$\langle A_T \rangle = \frac{l^2}{2v} - \frac{Dl}{v^2} \tanh\left(\frac{vl}{2D}\right). \quad (54)$$

Moreover, one can also show that for $X_0 > 0$, $D = 1/2$ and $v < 0$, till the first-passage time to the origin, which is equivalent to take $l_- \rightarrow 0$ and $l_+ \rightarrow \infty$ yields $\langle X_T^m \rangle \rightarrow 0$ and then $\langle A_T \rangle = (X_0^2/2v) + (X_0/2v^2)$, which was derived in previous works [16, 24].

Figure 2 illustrates the mean value of the area $\langle A_T \rangle$ (scaled by v^3/D^2) swept by the process X_t until time T , highlighting its dependence on the characteristic Péclet numbers. Simulation results (symbols) reproduce the analytical result Eq. (50) (lines) with exquisite accuracy. Two distinct cases are explored: the effect of increasing l_+ while maintaining l_- fixed at the values of $\text{Pe}^- = 2$ in panel A and $\text{Pe}^- = 2.5$ in panel B (red symbols and solid lines); and the effect of increasing l_- while keeping l_+ fixed at the values of $\text{Pe}^+ = 2$ in panel A and $\text{Pe}^+ = 2.5$ in panel B (blue symbols and dash-dotted lines). First, we analyze what happens when varying Pe^+ at constant Pe^- . Interestingly, the mean area decreases to negative values for smaller Pe^+ values, mainly because when $l_- \gg l_+$, negative contributions hold substantial weight. However, with increasing Pe^+ , $\langle A_T \rangle$ reaches a minimum and positive contributions become more significant due to the dominance of the positive bias as we have $v > 0$. This influence also leads to increasing the mean area with further increase in Pe^+ . Such non-monotonicity observed in the mean area $\langle A_T \rangle$ arises due to the competing behavior of two components $A_T^+ \equiv \int_0^T ds X_s \Theta(X_s)$ and $A_T^- \equiv \int_0^T ds X_s (1 - \Theta(X_s))$, where $\Theta(x)$ represents the Heaviside function. The quantities A_T^+ and A_T^- (referred to as positive and negative components of the area, respectively) denote the integrated area under the trajectory $X_{[0,T]}$ on the upper and lower halves of the axis $X_t = 0$, respectively (see Fig. 1). Consequently, the total area is given by $A_T = A_T^+ + A_T^-$ with $A_T^+ \geq 0$ and $A_T^- \leq 0$. When we increase Pe^+ at constant Pe^- , the positive component of the area keeps increasing while the negative one is exhausted reaching a saturation value. For smaller values of Pe^+ with fixed Pe^- , the mean area $\langle A_T \rangle$ is primarily influenced by the negative contribution of $\langle A_T^- \rangle$ as $\langle A_T^+ \rangle$ remains negligible. With further increments in Pe^+ , the positive contributions to $\langle A_T \rangle$ become significant as $\langle A_T^+ \rangle$ increases rapidly due to positive drift, leading to the minimum of $\langle A_T \rangle$. For larger values of Pe^+ , the average $\langle A_T^- \rangle$ reaches

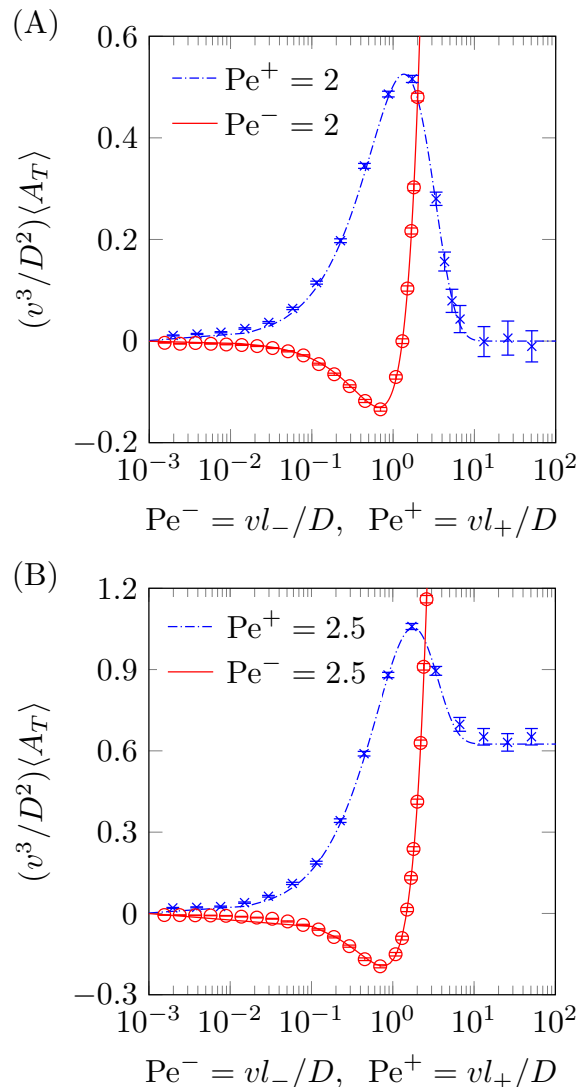


FIG. 2. Mean value of the area $\langle A_T \rangle$ swept by a biased diffusion (scaled by v^3/D^2 and with initial position $X_0 = 0$) till its first-exit time from the interval $(-l_-, l_+)$ as a function of the characteristic Péclet numbers. Simulation results (symbols) are compared with analytical results given by Eq. (50) (lines). Red symbols and solid lines show the effect of increasing Pe^+ while keeping Pe^- constant ($\text{Pe}^- = 2$ in panel A and $\text{Pe}^- = 2.5$ in panel B) and blue symbols and dash-dotted lines show the effect of increasing Pe^- as keeping Pe^+ constant ($\text{Pe}^+ = 2$ in panel A and $\text{Pe}^+ = 2.5$ in panel B). Note that in the asymptotic limit $v^3/D^2 \langle A_T \rangle$ tends to approach the value $[(\text{Pe}^+)^2 - 2\text{Pe}^+]/2$. Error bars show the standard error of the mean. Simulation parameters: number of stochastic realizations 10^4 , simulation time step 10^{-4} , and $v = D = 1$.

a saturation value due to fixed Pe^- , whereas $\langle A_T^+ \rangle$ continues to rise because of the positive drift. Numerical results illustrate the behavior of $\langle A_T^+ \rangle$, $\langle A_T^- \rangle$, and $\langle A_T \rangle$ with increasing Pe^+ at fixed Pe^- in panel (A) of Fig. 3.

We now analyze the behavior of the scaled mean area with varying Pe^- at constant Pe^+ , i.e., the dash-dotted

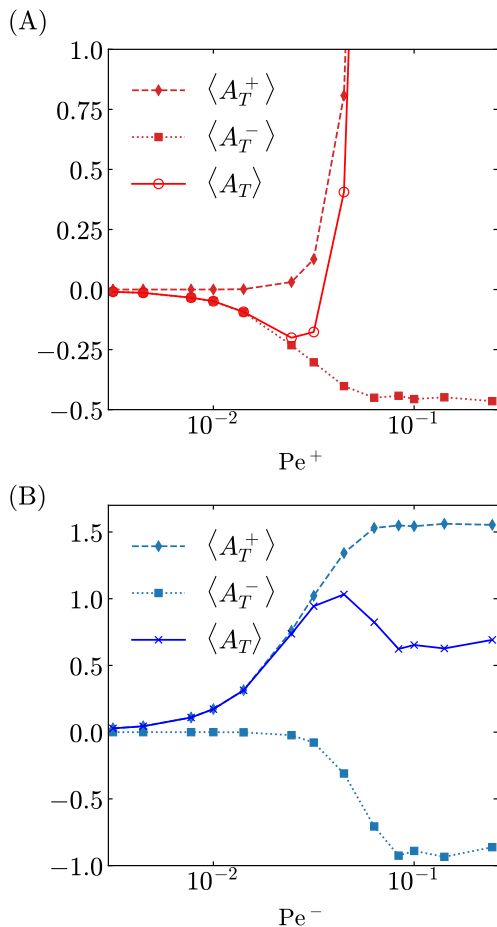


FIG. 3. Numerical estimates of $\langle A_T^+ \rangle$, $\langle A_T^- \rangle$ and $\langle A_T \rangle$ as a function of the characteristic Péclet numbers, obtained from numerical simulations. (A) Varying Pe^+ with Pe^- fixed at 2.5. (B) Varying Pe^- with Pe^+ fixed at 2.5. Symbols are obtained from numerical simulations, whereas the lines are guide to the eye. Simulation parameters: number of stochastic realizations 10^4 , simulation time step 10^{-4} , and $v = D = 1$.

blue lines in Fig. 2. The mean area starts increasing for smaller Pe^- values reaching a maximum. This trend again may be attributed to the interplay between the two distinct Péclet numbers in the system. For smaller values of Pe^- with fixed Pe^+ , $\langle A_T^- \rangle$ is negligible and the effect of the positive bias initially leads to an increase in $\langle A_T \rangle$ as the latter is dominated by $\langle A_T^+ \rangle$. See panel (B) in Fig. 3. With further increments in Pe^- , trajectories that move against the bias sweep more space below the time axis, which increases the magnitude of $\langle A_T^- \rangle$ and adds negative contributions to $\langle A_T \rangle$. This negative contribution along with the positive contribution from $\langle A_T^+ \rangle$ leads to the non-monotonicity of $\langle A_T \rangle$. For larger value of Pe^- , both $\langle A_T^+ \rangle$ and $\langle A_T^- \rangle$ reach saturation values (see panel (B) in Figure 3). The saturation of $\langle A_T^+ \rangle$ occurs because of fixed Pe^+ . On the other hand, the saturation of $\langle A_T^- \rangle$ arises because the trajectories eventually reach the positive threshold due to the large distance to the negative

threshold. Finally, the scaled mean area for large Pe^- with fixed Pe^+ saturates to the value $[(Pe^+)^2 - 2Pe^+]/2$.

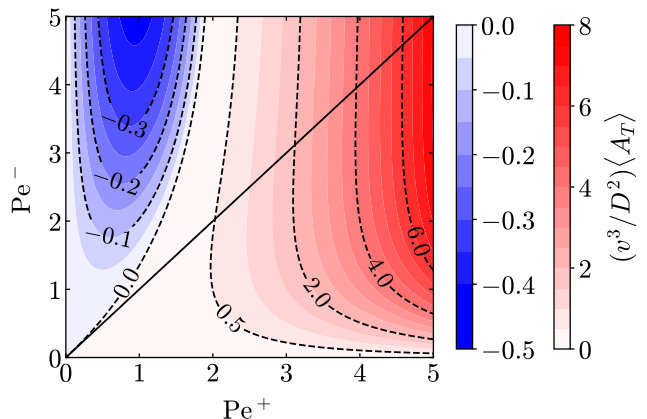


FIG. 4. Scaled mean area $(v^3/D^2)\langle A_T \rangle$ swept by a biased diffusion above the time axis till its first exit time from an interval as function of the characteristic Péclet numbers Pe^+ and Pe^- . The colormap shows analytical results obtained from Eq. (50). The solid black line has slope one, representing the region of symmetric absorbing boundaries. The dashed lines correspond to isolines for different values of the scaled mean area.

Figure 4 displays the analytical value of the mean area $\langle A_T \rangle$ as a function of both Pe^+ and Pe^- , suggesting that the mean area is strongly influenced by the bias. The colormap in Fig. 4 illustrates the impact of asymmetric absorbing boundaries on the mean area $\langle A_T \rangle$ as given by Eq. (50). Interestingly, in the region where Pe^+ and Pe^- are equal (indicated by the solid black line), the absorbing boundaries are symmetric, and the mean area is always positive, see Eq. (54). It is also worth noticing that there exists a region (between the solid black line with slope one and the dashed black line depicting $\langle A_T \rangle = 0$), in which the positive threshold is closer than the negative one $l_+ < l_-$ but yet the mean area is positive. We attribute this effect to the fact that the system is biased towards l_+ . This bias results in a greater accumulation of area in the positive region, and a correspondingly smaller area in the negative region. This difference is particularly pronounced at large values of Pe^+ , where the area becomes significantly larger than the corresponding area at large Pe^- values.

As a concluding note, we attack a hitherto unexplored quantity to our knowledge, by computing the cross-correlation function $C(X_T, T)$ between the first-exit time T and the exit site X_T . To this aim, we apply Doob's OSTm to a wisely-chosen Dynkin's martingales, and make use of our analytical expression for the mean area, together with previous knowledge on first-passage theory [47]. Identifying the Dynkin martingale associated with the function $g_t(x) = tx$ [see Eq. (11)] as $\mathcal{Y}_t = tX_t - \int_0^t ds(X_s + vt) = tX_t - A_t - vt^2/2$, and subsequently applying Doob's OSTm, i.e., $\langle \mathcal{Y}_T \rangle = \langle \mathcal{Y}_0 \rangle = 0$,

we obtain

$$\langle X_T T \rangle = \langle A_T \rangle + \frac{v \langle T^2 \rangle}{2}, \quad (55)$$

which holds for any stopping time that obeys conditions I and II in Sec. II A. Equation (55) implies that

$$\langle X_T T \rangle = \frac{v}{2} \langle T^2 \rangle - \frac{D \langle T \rangle}{v} + \frac{\langle X_T^2 \rangle - X_0^2}{2v}, \quad (56)$$

where we have used Eq. (49). Note that Eq. (56) is the same as Eq. (15), which is obtained from the Doléans–Dade exponential family. Using Eqs. (14) and (56), the

cross-correlation function $C(X_T, T) = \langle X_T T \rangle - \langle X_T \rangle \langle T \rangle$ may then be written as

$$C(X_T, T) = \frac{v}{2} \left(\langle T^2 \rangle - 2 \langle T \rangle^2 \right) - \left(X_0 + \frac{D}{v} \right) \langle T \rangle + \frac{\langle X_T^2 \rangle - X_0^2}{2v}, \quad (57)$$

which depends on the first and second moments of T and the second moment of X_T .

In particular, for the case of two absorbing boundaries positioned asymmetrically around the origin, we may use the corresponding expressions for $\langle T \rangle$, $\langle T^2 \rangle$, and $\langle X_T^2 \rangle$ in Eq. (57) (see Supplemental Material Sec. S1) and obtain

$$C(X_T, T) = \left(\frac{D^2}{v^3} \right) \frac{\exp(\text{Pe}^+) (\text{Pe}^- + \text{Pe}^+)}{\{\exp(\text{Pe}^+ + \text{Pe}^-) - 1\}^2} \left[\text{Pe}^+ \{\exp(\text{Pe}^-) - 1\} \{\exp(\text{Pe}^+) + 1\} - \text{Pe}^- \{\exp(\text{Pe}^-) + 1\} \{\exp(\text{Pe}^+) - 1\} \right]. \quad (58)$$

Equation (58) may be put in the scaling form

$$C(X_T, T) = \frac{D^2}{v^3} \Psi_C(\text{Pe}^+, \text{Pe}^-), \quad (59)$$

with the scaling function in this case given by

$$\Psi_C(x, y) = \frac{\exp(x)(x+y)}{[\exp(x+y) - 1]^2} \left[(\exp(y) - 1)(\exp(x) + 1)x - (\exp(y) + 1)(\exp(x) - 1)y \right]. \quad (60)$$

Figure 5 shows the analytical value of the scaled cross-correlation function $(v^3/D^2)C(X_T, T)$ [Eq. (58)] as a function of the characteristic Péclet numbers Pe^+ and Pe^- . The black line with a slope of one represent the region associated with symmetric absorbing boundaries, indicating that only within this region X_T and T are uncorrelated, i.e. $C(X_T, T) = 0$. This result is in agreement with the cross-correlation symmetry conjectured in Sec. II E. Unlike for the mean area $\langle A_T \rangle$, the cross-correlation function $C(X_T, T)$ is symmetric around the region $\text{Pe}^+ = \text{Pe}^-$, with the latter being a separatrix between two distinct regimes. When $\text{Pe}^+ > \text{Pe}^-$, there exists a positive correlation between the exit site and the exit time, whereas when $\text{Pe}^- > \text{Pe}^+$ the exit site and the exit time are anticorrelated. From this analysis and our exact formula (58) we conclude that positive X_T – T cross-correlations take place in asymmetric escape problems with the largest threshold in the direction of the drift, whereas negative X_T – T cross-correlations appear when the the largest threshold is in the direction opposite to the net drift. Such analysis could be of particular interest in the study of binary decision making in biology and neuroscience [48–51]. In particular, pushing forward our theory to more complex dynamics may result

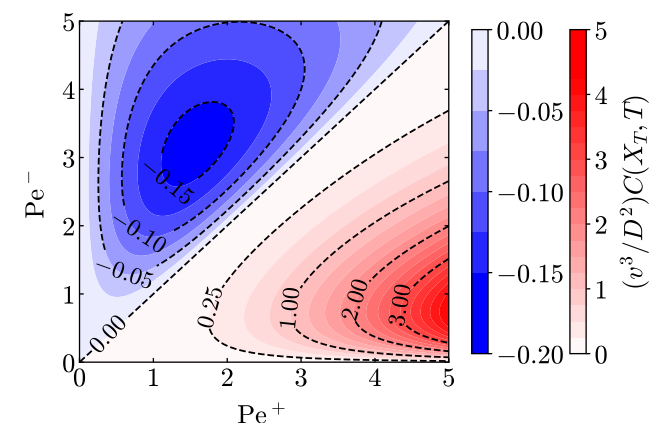


FIG. 5. Scaled cross-correlation function $(v^3/D^2)C(X_T, T)$ between the first-exit site X_T and the first-exit time T as function of the characteristic Péclet numbers Pe^+ and Pe^- . The colormap shows analytical results obtained from Eq. (59). Dashed lines represent isolines for different values of the scaled cross-correlation function. Note that the isoline corresponding to $(v^3/D^2)C(X_T, T) = 0$, where X_T and T are uncorrelated, has slope one representing the region of symmetric absorbing boundaries.

in inference schemes for the decision thresholds based on measurements of the cross-correlators $C(X_T, T)$.

V. CONCLUSIONS

Our work delves into the statistical analysis of one-dimensional biased diffusion governed by the overdamped

Langevin equation. Specifically, we have focused on the dynamics within an interval and investigated first-exit-time statistics, shedding light on various key aspects of the process. We have addressed the probability density $P(T)$ for the first exit time T from an interval. We have also examined the splitting probabilities for the particle to exit from the interval and the correlation between the first-exit time and the corresponding first-exit position. Incorporating tools from martingale theory, our approach enables the derivation of analytical results in first-passage theory. Notably, our calculations yield concise outcomes compared to traditional methods, such as path integrals and Fokker-Planck equations. Moreover, we have extended our analysis to the stochastic area swept by the biased diffusion for any class of stopping time, encompassing first-exit time as a specific example, contributing to the generalization of previous results in the literature. Finally, we have established general relations between moments and cross-correlations for any class of stopping times. In essence, our work not only presents a comprehensive study of biased diffusion dynamics within bounded intervals but also offers analytical shortcuts and broad insights into the statistical properties of first-exit times, positions, and associated stochastic areas. The utilization of martingale theory becomes a powerful tool in unraveling the intricacies of these stochastic processes, opening new doors for better understanding and further advancements of diffusion phenomena.

Besides statistical physics and decision theory, our results could have impact even in picturesque fields such as game theory and gambling. Suppose a gambler bets on the first-exit site of a drifted Brownian particle with negative drift $v < 0$, with its wealth in each game being to exit site value X_T . Then, no matter which threshold values l_+ and l_- he/she chooses, the game will lead to a net loss $\langle X_T \rangle \leq 0$. If however, the gambler's prize is based upon the area (i.e. the value of the time-integrated value of the particle position) then it is possible to find gambling strategies such that the net wealth $\langle A_T \rangle > 0$. Such strategies may be borrowed from the results in Sec. IV by just repeating the calculations but for the case $v < 0$. Even if reminiscent of Parrondo's paradoxical games [52], here the winning strategies do not require the switch between two strategies but rather just quitting the game at wisely-chosen threshold values l_+ and l_- . Furthermore, we expect such *winning* stopping strategies to inspire energy-extraction protocols in stochastic thermodynamics [53–55].

SUPPLEMENTAL MATERIAL

S1. MOMENTS OF THE FIRST-EXIT TIME AND THE FIRST-EXIT SITE FROM AN ASYMMETRIC INTERVAL OR ARBITRARY LENGTH

We examine the case of two absorbing boundaries located at $-l_-$ and l_+ with $l_{\pm} \geq 0$ for the process X_t given in Eq. (1). Here, the stopping time is given by $T = \inf\{t \geq 0 | X_t \notin [-l_-, l_+]\}$ with $X_0 = 0$. Henceforth, we will employ the notation, $\exp(x) = e^x$, in order to ensure clarity. The first moment of the stopping time T is given by Eq. (21), $\langle T \rangle = (l_+ P_+ - l_- P_-)/v$. By substituting Eq. (19) in Eq. (21), we obtain the first moment of the exit time as

$$\langle T \rangle = \frac{D \left[\text{Pe}^- + e^{\text{Pe}^+} \left(e^{\text{Pe}^-} \text{Pe}^+ - \text{Pe}^- - \text{Pe}^+ \right) \right]}{v^2 \left(e^{\text{Pe}^- + \text{Pe}^+} - 1 \right)}. \quad (\text{S1})$$

Equation (S1) may be also obtained using the relation [47]

$$\langle T \rangle (X_0) = \frac{1}{D} \left[\int_{X_0}^{l_+} d\eta \pi(\eta) \int_{-l_-}^{\eta} (\pi(\xi))^{-1} d\xi - R(X_0) \int_{-l_-}^{l_+} d\eta \pi(\eta) \int_{-l_-}^{\eta} (\pi(\xi))^{-1} d\xi \right], \quad (\text{S2})$$

where $\langle T \rangle (X_0)$ denotes the mean exit time as a function of the initial position X_0 , and we have $\pi(y) \equiv \exp(-vy/D)$ and $R(X_0) \equiv (\exp(\text{Pe}^+ - vX_0/D) - 1) / (\exp(\text{Pe}^+ + \text{Pe}^-) - 1)$. In general, the n -th moment of the exit time may be written as [47]

$$\langle T^n \rangle (X_0) = \frac{n}{D} \left[\int_{X_0}^{l_+} d\eta \pi(\eta) \int_{-l_-}^{\eta} \frac{\langle T^{n-1} \rangle (\xi)}{\pi(\xi)} d\xi - R(X_0) \int_{-l_-}^{l_+} d\eta \pi(\eta) \int_{-l_-}^{\eta} \frac{\langle T^{n-1} \rangle (\xi)}{\pi(\xi)} d\xi \right]. \quad (\text{S3})$$

In particular, for $X_0 = 0$, the second moment of the exit time obtained by substituting Eq. (S2) in Eq. (S3) reads

$$\begin{aligned} \langle T^2 \rangle = \frac{D^2}{v^4 \left(e^{\text{Pe}^- + \text{Pe}^+} - 1 \right)^2} & \left[\left(e^{\text{Pe}^-} - 1 \right) e^{\text{Pe}^+} (\text{Pe}^+)^2 \left(e^{\text{Pe}^- + \text{Pe}^+} + 3 \right) - (\text{Pe}^-)^2 \left(e^{\text{Pe}^+} - 1 \right) \left(3e^{\text{Pe}^- + \text{Pe}^+} + 1 \right) \right. \\ & + 2 \left(e^{\text{Pe}^- + \text{Pe}^+} - 1 \right) \left\{ \text{Pe}^- - e^{\text{Pe}^+} \left(-e^{\text{Pe}^-} \text{Pe}^+ + \text{Pe}^- + \text{Pe}^+ \right) \right\} \\ & \left. - 4\text{Pe}^- \text{Pe}^+ \left(-2e^{\text{Pe}^- + \text{Pe}^+} + e^{\text{Pe}^- + 2\text{Pe}^+} + e^{\text{Pe}^+} \right) \right]. \quad (\text{S4}) \end{aligned}$$

The m -th moment of X_T is given by Eq. (20), $\langle X_T^m \rangle = (-l_-)^m P_- + l_+^m P_+$. Using Eq. (19) in the latter expression, we retrieve the first two moments of the exit site for the case $X_0 = 0$

$$\langle X_T \rangle = \frac{D \left[\text{Pe}^- + e^{\text{Pe}^+} \left(e^{\text{Pe}^-} \text{Pe}^+ - \text{Pe}^- - \text{Pe}^+ \right) \right]}{v \left(e^{\text{Pe}^- + \text{Pe}^+} - 1 \right)}, \quad (\text{S5})$$

$$\langle X_T^2 \rangle = \frac{D^2 \left[\left(e^{\text{Pe}^+} - 1 \right) (\text{Pe}^-)^2 + \left(e^{\text{Pe}^-} - 1 \right) e^{\text{Pe}^+} (\text{Pe}^+)^2 \right]}{v^2 \left(e^{\text{Pe}^- + \text{Pe}^+} - 1 \right)}. \quad (\text{S6})$$

- [1] Robert Brown. XXVII. A brief account of microscopical observations made in the months of June, July and August 1827, on the particles contained in the pollen of plants; and on the general existence of active molecules in organic and inorganic bodies. *The Philosophical Magazine*, 4(21):161–173, 1828.
- [2] Albert Einstein et al. On the motion of small particles suspended in liquids at rest required by the molecular-kinetic theory of heat. *Annalen der physik*, 17(549-560):208, 1905.
- [3] Jean Perrin. *Brownian Movement and Molecular Reality*. Courier Corporation, 2013.
- [4] Ryogo Kubo. Brownian Motion and Nonequilibrium Statistical Mechanics. *Science*, 233(4761):330–334, 1986.
- [5] Peter Hänggi and Fabio Marchesoni. Introduction: 100 years of Brownian motion. *Chaos*, 15(2):026101, 2005.

- [6] George K. Batchelor. The effect of brownian motion on the bulk stress in a suspension of spherical particles. *Journal of Fluid Mechanics*, 83(1):97–117, 1977.
- [7] Jan Mewis and Norman J. Wagner. *Colloidal Suspension Rheology*. Cambridge University Press, Cambridge, 2011.
- [8] Ruslan L. Stratonovich. *Topics in the Theory of Random Noise*. Gordon and Breach, 1963.
- [9] Edward Nelson. *Dynamical Theories of Brownian Motion*. Mathematical Notes. Princeton University Press, 1967.
- [10] Crispin Gardiner. *Handbook of Stochastic Methods for Physics, Chemistry, and the Natural Sciences*. Springer, Berlin, 2004.
- [11] Fischer Black and Myron Scholes. The pricing of options and corporate liabilities. *Journal of Political Economy*, 81(3):637–654, 1973.
- [12] Thomas G. Mason and David. A. Weitz. Optical measurements of frequency-dependent linear viscoelastic moduli of complex fluids. *Physical Review Letters*, 74:1250–1253, 1995.
- [13] Crispin Gardiner and Peter Zoller. *Quantum Noise: A Handbook of Markovian and Non-Markovian Quantum Stochastic Methods with Applications to Quantum Optics*. Springer, Berlin, 2004.
- [14] Michele Campisi, Peter Hänggi, and Peter Talkner. Colloquium: Quantum fluctuation relations: Foundations and applications. *Reviews of Modern Physics*, 83:771–791, 2011.
- [15] Satya N. Majumdar and Alain Comtet. Airy Distribution Function: From the area under a Brownian excursion to the maximal height of fluctuating interfaces. *Journal of Statistical Physics*, 119(3-4):777–826, May 2005.
- [16] Michael J. Kearney and Satya N. Majumdar. On the area under a continuous time brownian motion till its first-passage time. *Journal of Physics A: Mathematical and General*, 38(19):4097, 2005.
- [17] Michael J. Kearney, Satya N. Majumdar, and Richard J. Martin. The first-passage area for drifted brownian motion and the moments of the airy distribution. *Journal of Physics A: Mathematical and Theoretical*, 40(36):F863 – F869, 2007.
- [18] Michael J. Kearney and Satya N. Majumdar. Statistics of the first passage time of brownian motion conditioned by maximum value or area. *Journal of Physics A: Mathematical and Theoretical*, 47(46):465001, 2014.
- [19] Satya N. Majumdar. Brownian Functionals in Physics and Computer Science. *Current Science*, 89:2076, 2005.
- [20] Philippe Flajolet, Patricio Poblete, and Alfredo Viola. On the analysis of linear probing hashing. *Algorithmica*, 22(4):490–515, 1998.
- [21] Svante Janson. Brownian excursion area, Wright’s constants in graph enumeration, and other Brownian areas. *Probability Surveys*, 4:80 – 145, 2007.
- [22] Joseph L. Doob. *Stochastic Processes*. John Wiley & Sons, New York, 1990.
- [23] Édgar Roldán, Izaak Neri, Raphael Chetrite, Shamik Gupta, Simone Pigolotti, Frank Jülicher, and Ken Sekimoto. Martingales for physicists. *arXiv preprint arXiv:2210.09983*, 2022.
- [24] Mario Abundo. On the first-passage area of a one-dimensional jump-diffusion Process. *Methodology and Computing in Applied Probability*, 15(1):85–103, 2013.
- [25] Johan du Buisson, Thamu DP Mnyulwa, and Hugo Touchette. Large deviations of the stochastic area for linear diffusions. *Physical Review E*, 108(4):044136, 2023.
- [26] Naftali R. Smith. Anomalous scalings of fluctuations of the area swept by a brownian particle trapped in a $|x|$ potential. *arXiv preprint arXiv:2311.18366*, 2023.
- [27] Sidney Redner. *A Guide to First-Passage Processes*. Cambridge University Press, Cambridge, 2001.
- [28] Ralf Metzler, Gleb Oshanin, and Sidney Redner. *First-Passage Phenomena and Their Applications*. World Scientific, 2014.
- [29] Ken Sekimoto. Derivation of the First Passage Time Distribution for Markovian Process on Discrete Network, 2022. *arXiv:2110.02216* [cond-mat, physics:physics].
- [30] Francesco Avanzini, Massimo Bilancioni, Vasco Cavina, Sara Dal Cengio, Massimiliano Esposito, Gianmaria Falasco, Danilo Forastiere, Nahuel Freitas, Alberto Garilli, Pedro E. Harunari, Vivien Lecomte, Alexandre Lazarescu, Shesha G. Marehalli Srinivas, Charles Moslonka, Izaak Neri, Emanuele Penocchio, William D. Piñeros, Matteo Polettini, Adarsh Raghu, Paul Raux, Ken Sekimoto, and Ariane Soret. Methods and Conversations in (Post)Modern Thermodynamics, November 2023. *arXiv:2311.01250* [cond-mat].
- [31] Silvia Bartolucci, Fabio Caccioli, Francesco Caravelli, and Pierpaolo Vivo. Ranking influential nodes in networks from aggregate local information. *Physical Review Research*, 5(3):033123, 2023.
- [32] Talia Baravi and Eli Barkai. First passage times in compact domains exhibits bi-scaling. *arXiv preprint arXiv:2311.13915*, 2023.
- [33] Catherine Doléans-Dade. Quelques applications de la formule de changement de variables pour les semimartingales. *Zeitschrift für Wahrscheinlichkeitstheorie und verwandte Gebiete*, 16:181–194, 1970.
- [34] Philip E. Protter. *Stochastic Integration and Differential Equations*. Springer, Berlin, 2nd edition, 2004.
- [35] Raphaël Chetrite and Shamik Gupta. Two refreshing views of fluctuation theorems through kinematics elements and exponential martingale. *Journal of Statistical Physics*, 143:543–584, 2011.
- [36] Izaak Neri, Édgar Roldán, and Frank Jülicher. Statistics of infima and stopping times of entropy production and applications to active molecular processes. *Physical Review X*, 7:011019, 2017.
- [37] Evgenii B. Dynkin, A. A. Yushkevich, G. M. Seitz, and A. L. Onishchik. *Selected Papers of E. B. Dynkin with Commentary*. American Mathematical Society, Boston, 2000.
- [38] Édgar Roldán, Izaak Neri, Meik Dörpinghaus, Heinrich Meyr, and Frank Jülicher. Decision making in the arrow of time. *Physical Review Letters*, 115(25):250602, 2015.
- [39] Pavel L. Krapivsky and Sidney Redner. First-passage duality. *Journal of Statistical Mechanics: Theory and Experiment*, 2018(9):093208, 2018.

- [40] Meik Dörpinghaus, Izaak Neri, Édgar Roldán, Heinrich Meyr, and Frank Jülicher. Testing optimality of sequential decision-making. *arXiv preprint arXiv:1801.01574*, 2018.
- [41] Meik Dorpinghaus, Izaak Neri, E Roldán, and Frank Julicher. Optimal information usage in binary sequential hypothesis testing. *Theory of Probability & Its Applications*, 68(1):77–87, 2023.
- [42] X Sheldon Lin. Double barrier hitting time distributions with applications to exotic options. *Insurance: Mathematics and Economics*, 23(1):45–58, 1998.
- [43] Vaibhav Srivastava, Samuel F Feng, Jonathan D Cohen, Naomi Ehrich Leonard, and Amitai Shenhav. A martingale analysis of first passage times of time-dependent wiener diffusion models. *Journal of mathematical psychology*, 77:94–110, 2017.
- [44] Izaak Neri. Universal tradeoff relation between speed, uncertainty, and dissipation in nonequilibrium stationary states. *SciPost Physics*, 12(4):139, 2022.
- [45] George E. Roberts and Hyman Kaufman. *Table of Laplace Transforms*. W. B. Saunders Company, 1966.
- [46] Fritz Oberhettinger and Larry Badii. *Tables of Laplace transforms*. Springer, Berlin, 1973.
- [47] Narendra S. Goel and Nira Richter-Dyn. *Stochastic Models in Biology*. Academic Press, London, 1974.
- [48] Eric D. Siggia and Massimo Vergassola. Decisions on the fly in cellular sensory systems. *Proceedings of the National Academy of Sciences of the United States of America*, 110(39):E3704–E3712, 2013.
- [49] Jin Wang. Landscape and flux theory of non-equilibrium dynamical systems with application to biology. *Advances in Physics*, 64(1):1–137, 2015.
- [50] Wiet de Ronde, Pieter Rein ten Wolde, and Andrew Mugler. Protein logic: a statistical mechanical study of signal integration at the single-molecule level. *Biophysical Journal*, 103(5):1097–1107, 2012.
- [51] Aybüke Durmaz, Yonathan Sarmiento, Gianfranco Fortunato, Debraj Das, Mathew Ernst Diamond, Domenica Bueti, and Édgar Roldán. Human perceptual decision making of nonequilibrium fluctuations. *arXiv preprint arXiv:2311.12692*, 2023.
- [52] Juan MR Parrondo, Gregory P Harmer, and Derek Abbott. New paradoxical games based on brownian ratchets. *Physical Review Letters*, 85(24):5226, 2000.
- [53] Izaak Neri, Édgar Roldán, Simone Pigolotti, and Frank Jülicher. Integral fluctuation relations for entropy production at stopping times. *Journal of Statistical Mechanics: Theory and Experiment*, 2019(10):104006, 2019.
- [54] Gonzalo Manzano, Diego Subero, Olivier Maillet, Rosario Fazio, Jukka P Pekola, and Édgar Roldán. Thermodynamics of gambling demons. *Physical Review Letters*, 126(8):080603, 2021.
- [55] Haoran Yang and Hao Ge. Fluctuation theorems and thermodynamic inequalities for nonequilibrium processes stopped at stochastic times. *arXiv preprint arXiv:2306.00345*, 2023.